



HAL
open science

First-principles study of ultrafast bandgap dynamics in laser-excited

α

-quartz

Elena Kachan, Arshak Tsaturyan, Razvan Stoian, Jean-Philippe Colombier

► **To cite this version:**

Elena Kachan, Arshak Tsaturyan, Razvan Stoian, Jean-Philippe Colombier. First-principles study of ultrafast bandgap dynamics in laser-excited

α

-quartz. The European Physical Journal. Special Topics, 2023, 232 (13), pp.2241-2245. 10.1140/epjs/s11734-022-00747-8 . ujm-04244763

HAL Id: ujm-04244763

<https://ujm.hal.science/ujm-04244763v1>

Submitted on 16 Oct 2023

HAL is a multi-disciplinary open access archive for the deposit and dissemination of scientific research documents, whether they are published or not. The documents may come from teaching and research institutions in France or abroad, or from public or private research centers.

L'archive ouverte pluridisciplinaire **HAL**, est destinée au dépôt et à la diffusion de documents scientifiques de niveau recherche, publiés ou non, émanant des établissements d'enseignement et de recherche français ou étrangers, des laboratoires publics ou privés.

First-principles study of ultrafast bandgap dynamics in laser-excited α -quartz

Elena Kachan, Arshak Tsaturyan, Razvan Stoian and Jean-Philippe Colombier

*Univ Lyon, UJM-Saint-Etienne, CNRS, Institut d'Optique Graduate School, Laboratoire Hubert Curien UMR 5516, Saint-Etienne, France.

*Corresponding author(s). E-mail(s): elena.kachan@univ-st-etienne.fr;

Abstract

Femtosecond-laser-induced evolution of α -quartz bandgap was calculated using first principles. First, Time-Dependent Density Functional Theory (TDDFT) was used to describe excited electron dynamics during the laser pulse irradiation. Then the temperature of excited electrons was estimated using Finite-Temperature DFT. Finally, the \mathbf{GW} approximation was applied to calculate the electronic structure modification driven by hot electrons. As a result, an ultrafast decrease of the bandgap is observed during a 15-fs laser pulse with a drop of 35 % at laser intensities near the damage threshold.

Keywords: femtosecond laser pulse, bandgap, hot electrons, photoexcitation, α -quartz, first principles

1 Introduction

The studies of ultrafast laser-matter interaction in wide-bandgap insulators govern the progress of modern technologies such as optical data storage, integrated photonics, ultrafast signal processing etc [1–3]. The main challenge in optimizing experimental processes consists in a proper estimation of laser energy redistribution and photoexcitation rate as exotic strong-field phenomena appear on ultrashort timescales [4].

The main theory of strong-field ionization was developed by Keldysh in 1964 [5]. His non-perturbative method is now widely used to calculate the photoionization rates in wide-bandgap solids under ultrafast laser irradiation. Additional improvements were made by including non-parabolic band structure and collisional ionization process [6, 7]. These approaches consider unperturbed electronic states during the laser pulse. The strong photo-excitation can however affect the

band structure stability on ultrashort timescales with consequences for transient photoabsorption.

The attosecond bandgap dynamics was already observed in semiconductors [8] where electronic structure followed the laser electric field oscillations. The bandgap shrinkage of several electronvolts was also hypothesized to take place in photoexcited fused silica according to the experiments [2]. High electron temperature and thus high excited electron density leads to the bandgap decrease as predicted theoretically for various semiconductors and insulators [9]. In this paper, we combine Time-Dependent Density Functional Theory (TDDFT), finite-temperature DFT and \mathbf{GW} approximation to show that in α -quartz excited at damage-threshold intensities, the bandgap is drastically modified, confirming the previous hypotheses [2]. The obtained bandgap evolution can be used to further improve the photoionization control and better understand the transient optical properties.

2 Methods

Three different first-principles methods were combined to obtain the bandgap dynamics during a laser pulse: TDDFT, finite-temperature DFT and *GW* approximation. The details of each calculation are given below.

2.1 Real-time TDDFT

The real-time electron dynamics in α -quartz is calculated using TDDFT implemented in SALMON (Scalable Ab-initio Light-Matter simulator for Optics and Nanoscience) [10]. The evolution of the system is obtained by solving time-dependent equations for lattice-periodic Kohn-Sham orbitals $\psi_i(\mathbf{r}, t)$:

$$i\hbar \frac{\partial}{\partial t} \psi_i(\mathbf{r}, t) = \left[\frac{1}{2m_e} \left(-i\hbar \nabla + \frac{e}{c} \mathbf{A}(t) \right)^2 + V(\mathbf{r}, t) \right] \psi_i(\mathbf{r}, t), \quad (1)$$

where $V(\mathbf{r}, t)$ includes ionic, Hartree and exchange-correlation potentials. A meta-generalized-gradient approximation (meta-GGA) of Tran and Blaha is employed for exchange-correlation potential [11]. This potential is known to better reproduce the bandgaps of semiconductors and insulators. The spatially-uniform electric field of the laser pulse is introduced through vector potential $\mathbf{A}(t)$:

$$\mathbf{A}(t) = -\frac{cE_0\mathbf{e}}{\omega} \sin^2\left(\frac{\pi t}{\tau_L}\right) \cos(\omega t) \quad (2)$$

if $0 < t < \tau_L$ and 0 otherwise. The pulse duration τ_L is related to the usual full width at half-maximum intensity (FWHM) as $\tau_{\text{FWHM}} = 0.364\tau_L$. The peak electric field inside the crystal E_0 depends on peak electric field in vacuum E_v as $E_0 = 2E_v/(n+1)$ where n is the refractive index at laser frequency ω . The refractive index is assumed to change negligibly at given excitation levels [12]. The polarization unit vector \mathbf{e} is parallel to the c -axis of the crystal that coincides with z direction.

A uniform Cartesian grid with dimensions $20 \times 36 \times 52$ is applied to the rectangular unit cell containing 6 silicon atoms and 12 oxygen atoms. The

k -space is discretized into 4^3 grid points and a time step of 1 as is used.

The density of excited electrons $n_e(t)$ is defined from the projection of the time-dependent states $\psi_i(t)$ on the initial states $\psi_i(0)$:

$$n_e(t) = \frac{1}{\Omega} \sum_{ii'=\text{occ}} (\delta_{ii'} - |\langle \psi_i(0) | \psi_{i'}(t) \rangle|^2), \quad (3)$$

where the sum runs over initially occupied states and Ω is the unit cell volume.

The excited electrons thermalize rapidly and their thermal distribution follows Fermi-Dirac statistics [13]. The TDDFT with meta-GGA functional however does not treat properly electron-electron relaxation and only partial thermalization is possible due to ion-electron interaction under laser field [14, 15]. Moreover, the excited electron screening effects leading to the bandgap renormalization are underestimated. To overcome these limitations, we used a finite-temperature DFT with *GW* bandgap correction [9]. Similar approach was used previously to describe the silicon bandgap dynamics [8].

2.2 Finite-temperature DFT

Finite-temperature DFT was used to obtain a relation between electron temperature and excited electron density. In case of the DFT calculations with a thermal ensemble of electrons, the Kohn-Sham equations for static orbitals $\phi_i(\mathbf{r})$ are given by

$$\left[-\frac{\hbar^2}{2m_e} \nabla^2 + V(\mathbf{r}) \right] \phi_i(\mathbf{r}) = \epsilon_i \phi_i(\mathbf{r}). \quad (4)$$

The potential $V(\mathbf{r})$ is a function of electron density defined by Fermi-Dirac distribution of electrons over orbital energies ϵ_i :

$$f_i = \frac{1}{1 + e^{(\epsilon_i - \mu)/k_B T_e}} \quad (5)$$

where μ is the chemical potential and $k_B T_e$ is the electron temperature in energy units. At $T_e = 0$ the conduction band is empty. Higher T_e corresponds to the electron excitation and the conduction band becomes filled with electrons. Thus, a dependence of the excited-electron density as a function of T_e can be found.

Equations 4 are solved using the SALMON package with the same unit cell parameters and

meta-GGA potential as in section 2.1. The k -space grid is denser with 8^3 points.

The DFT does not properly take into account many-body effects due to electron-electron interactions. It thus shows a universal increase of the bandgap as a function of electron temperature [9]. The bandgap narrowing is however expected with the increase of conduction electron density [16, 17] and can be reproduced using GW formalism [9].

2.3 GW approximation

The bandgap of α -quartz as a function of electron temperature is calculated using GW approximation of the many-body perturbation theory implemented in the ABINIT software [18]. The quasi-particle self-consistent GW method is applied in the calculation. In this method, the quasi-particle energy ϵ^{QP} is expressed as the energy eigenvalue ϵ obtained from DFT Kohn-Sham equations (Eqs. 4) plus a many-body correction:

$$\epsilon^{\text{QP}} = \epsilon + \frac{\langle \phi | \Sigma(\epsilon) - v_{\text{xc}} | \phi \rangle}{\left[1 - \langle \phi | \frac{\partial \Sigma(\epsilon)}{\partial \epsilon} | \phi \rangle \right]} \quad (6)$$

where v_{xc} is the exchange-correlation potential and self-energy $\Sigma(\epsilon)$ is calculated from the Green's function G and screened Coulomb interaction W . The screening is described by a plasmon-pole approximation of the dielectric response function [19]. The initial hamiltonian used in Eqs. 4 is then further improved through a GW self-consistent procedure.

The initial energy eigenvalues are calculated using DFT with Perdew-Burke-Ernzerhof GGA of exchange-correlation functional and PAW atomic data treating $3s^23p^2$ and $2s^22p^4$ valence electrons for Si and O, respectively. A plane-wave cutoff energy of 816 eV and a 4^3 k-point grid is used. The number of bands and cutoff energy for self-energy calculations are set to 200 and 272 eV, respectively. The cutoff energy for screening calculations is set to 408 eV.

3 Results

The material is irradiated by a 15-fs (FWHM) laser pulse at 800 nm wavelength (1.55 eV photon energy) and near-damage fluence of 2.2 J/cm^2 . Such fluence corresponds to the intensity inside

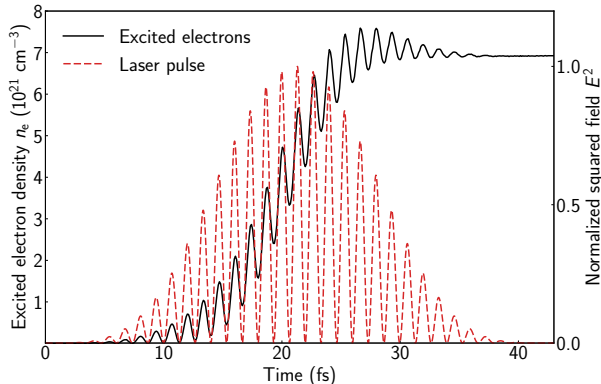


Fig. 1 Evolution of excited electron density (solid line) and normalized squared laser electric field E^2 (dashed line) inside α -quartz irradiated by a laser pulse with 15-fs pulse duration, fluence 2.2 J/cm^2 and wavelength 800 nm, calculated using TDDFT.

material of $9 \times 10^{13} \text{ W/cm}^2$ considering the refractive index $n = 1.45$ at 800 nm. The density of electrons excited into the conduction band predicted by TDDFT calculations is shown in Fig. 1. The excited electron density increases in time following the oscillations of squared field $E^2(t)$ and reaches about $7 \times 10^{21} \text{ cm}^{-3}$ in the end of the laser pulse.

The density of the excited electrons is directly related to their temperature as shown in Fig. 2. This dependence results from Fermi-Dirac distribution (Eq. 5) used in finite-temperature DFT and can be fitted by the Boltzmann approximation :

$$n_e = A e^{-E_a/k_B T_e} \quad (7)$$

with fitting parameters $A = 140.7 \times 10^{21} \text{ cm}^{-3}$ and $E_a = 5.8 \text{ eV}$. Although, the electrons in TDDFT are not perfectly thermalized to Fermi-Dirac distribution during the laser pulse [15], the equation 7 can be used to obtain an effective electron temperature from TDDFT excited electron density shown in Fig. 1. The evolution of the effective electron temperature, obtained in this way, recovers the oscillations of the electron density observed in TDDFT results (Fig. 3). Such sub-femtosecond dynamics of electron temperature is however questionable because excited electrons need time to reach thermal equilibrium [13]. To reproduce the delayed response of electron temperature the oscillations are smoothed using a moving-average filter. The maximum electron temperature reached after the laser pulse is thus 1.9 eV.

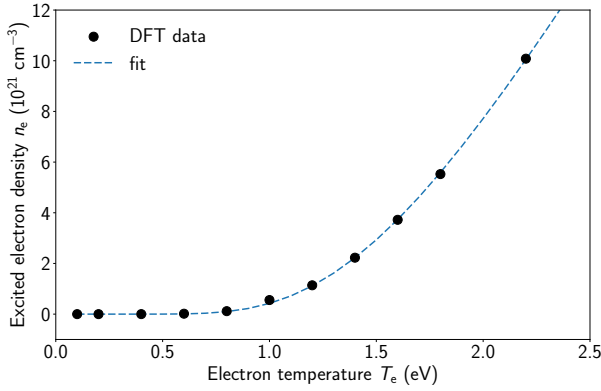


Fig. 2 Excited electron density n_e as a function of electron temperature T_e predicted by finite-temperature DFT and an Arrhenius fit (Eq. 7).

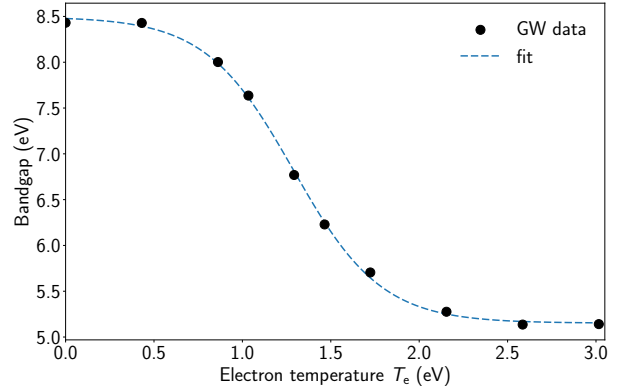


Fig. 4 Bandgap as function of electron temperature predicted by GW approximation with interpolation curve obtained using Eq. 8.

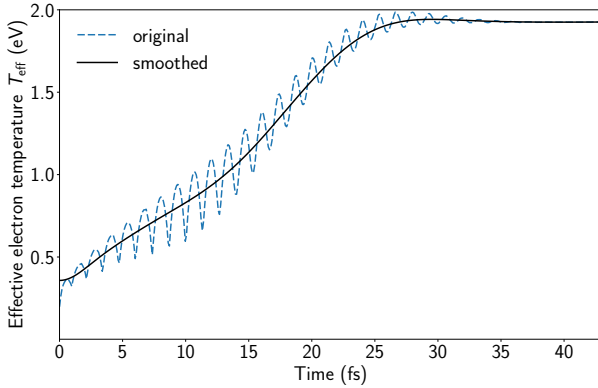


Fig. 3 Effective electron temperature evolution during the laser pulse shown in Fig. 1 with superimposed original and smoothed data.

Previously, the bandgap reduction with increasing T_e and slower behavior at larger T_e was observed for different semiconductors and insulators [9]. The same behavior is obtained for α -quartz using GW approximation and shown in Fig. 4. The calculated bandgap decreases by more than 3 eV at $T_e = 3$ eV. Note that a bandgap of 8.4 eV is obtained at zero temperature close to the previous GW results and experiments, reporting values around 9 eV [20, 21]. The following equation is fitted to the GW data to obtain a smooth interpolation:

$$E_g = 5.15 + \frac{3.34}{1 + e^{(T_e - 1.29)/0.25}} \quad (8)$$

The equation 8 is then combined with T_e time-dependence shown in Fig. 3 and the bandgap evolution during the laser pulse is finally obtained

(Fig. 5). The bandgap decreases rapidly during the laser pulse and drops down below 5.5 eV from initial 8.4 eV at a fluence of 2.2 J/cm². A decrease of 1 eV is observed after the laser pulse with 1 J/cm² fluence. Note also that at lower fluence the bandgap has a small minimum just after the laser peak. It is related to a transient peak of electron density caused by a virtual energy transfer from the laser pulse to electrons of transparent insulators at low laser intensities [22].

One should keep in mind that the relation between excited electron density and electron temperature, obtained from DFT, can be slightly different due to GW corrections of the band structure. Due to the task complexity, we did not extract this information from GW calculation and thus a certain error is expected when the electron temperature is used to relate the electron densities in GW and TDDFT calculations.

Despite certain limitations of the presented methods (non-equilibrium electrons in TDDFT and excited electron density uncertainties due to GW correction), the bandgap drop obtained at the end of the laser pulse is on the same order of magnitude as the one predicted by the experiments on fused silica (see supplementary materials of Ref. [2]). In Ref. [2], the bandgap decrease from 9 eV to 6 eV is expected after the irradiation by a 30-fs laser pulse at 800-nm wavelength and 1.2 J/cm² fluence.

The bandgap narrowing observed in this work is caused purely by the change of electron-electron interaction at high electron temperatures. Additional bandgap decrease is expected from

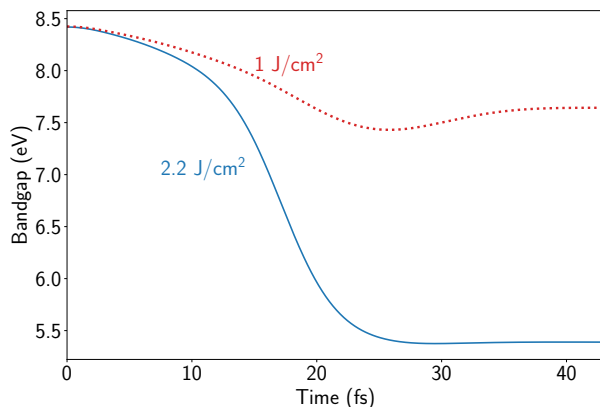


Fig. 5 Bandgap evolution during 15-fs (FWHM) laser pulse at 800-nm wavelength and two fluences 2.2 J/cm² (solid line) and 1 J/cm² (dotted line).

excitation-induced atomic displacements [23, 24] but might happen at longer time delays. Moreover, the laser-dressed electronic structure can experience a bandgap collapse, although this process is transient and is not maintained after the end of the laser pulse [25].

4 Conclusions

The α -quartz bandgap evolution during femtosecond laser irradiation is calculated using first principles. The initial bandgap of 8.4 eV decreases rapidly down to 7.6 eV (10 % drop) at 1 J/cm² fluence and down to 5.4 eV (35 % drop) at 2.2 J/cm² on a timescale of a 15-fs laser pulse. The bandgap narrowing is caused by a strong increase of conduction electron density and their high temperature during laser excitation. This result highlights the importance of taking into account the transient electronic and optical properties when estimating laser energy transfer in wide-bandgap solids after the laser pulse. The bandgap decrease of several electronvolts is comparable to the photon energy and thus changes drastically the photoexcitation rate as strongly nonlinear multiphoton ionization processes are involved.

Acknowledgements The numerical calculations were performed using computer resources from GENCI, project gen7041.

Funding The work was funded by IDEX-LYON project of the University of Lyon within

the program "Investissements d'Avenir" (ANR-16-IDEX-0005) and INTRALAS project (ANR-19-CE30-0036) operated by the French National Research Agency (ANR).

Data availability The datasets generated during the current study are available from the corresponding author on reasonable request.

References

- [1] Schiffrin, A., Paasch-Colberg, T., Karpowicz, N., Apalkov, V., Gerster, D., Mühlbrandt, S., Korbman, M., Reichert, J., Schultze, M., Holzner, S., Barth, J.V., Kienberger, R., Ernstorfer, R., Yakovlev, V.S., Stockman, M.I., Krausz, F.: Optical-field-induced current in dielectrics. *Nature* **493**(7430), 70 (2013)
- [2] Winkler, T., Haahr-Lillevang, L., Sarpe, C., Zielinski, B., Götze, N., Senftleben, A., Balling, P., Baumert, T.: Laser amplification in excited dielectrics. *Nature Phys.* **14**(1), 74 (2018)
- [3] Stoian, R.: Volume photoinscription of glasses: three-dimensional micro- and nanostructuring with ultrashort laser pulses. *Appl. Phys. A* **126**(6), 438 (2020)
- [4] Kruchinin, S.Y., Krausz, F., Yakovlev, V.S.: Colloquium: Strong-field phenomena in periodic systems. *Rev. Mod. Phys.* **90**(2), 021002 (2018)
- [5] Keldysh, L.V.: Ionization in the field of a strong electromagnetic wave. *Sov. Phys. JETP* **20**, 1307 (1965)
- [6] Gruzdev, V.E.: Photoionization rate in wide band-gap crystals. *Phys. Rev. B* **75**(20), 205106 (2007)
- [7] Rethfeld, B.: Unified model for the free-electron avalanche in laser-irradiated dielectrics. *Phys. Rev. Lett.* **92**(18), 187401 (2004)
- [8] Schultze, M., Ramasesha, K., Pemmaraju, C.D., Sato, S.A., Whitmore, D., Gandman, A., Prell, J.S., Borja, L.J., Prendergast, D., Yabana, K., Neumark, D.M., Leone, S.R.:

- Attosecond band-gap dynamics in silicon. *Science* **346**(6215), 1348 (2014)
- [9] Faleev, S.V., van Schilfgaarde, M., Kotani, T., Léonard, F., Desjarlais, M.P.: Finite-temperature quasiparticle self-consistent *GW* approximation. *Phys. Rev. B* **74**(3), 033101 (2006)
- [10] Noda, M., Sato, S.A., Hirokawa, Y., Uemoto, M., Takeuchi, T., Yamada, S., Yamada, A., Shinohara, Y., Yamaguchi, M., Iida, K., Floss, I., Otobe, T., Lee, K.-M., Ishimura, K., Boku, T., Bertsch, G.F., Nobusada, K., Yabana, K.: SALMON: Scalable Ab-initio Light-Matter simulator for Optics and Nanoscience. *Comput. Phys. Commun.* **235**, 356 (2019)
- [11] Tran, F., Blaha, P.: Accurate band gaps of semiconductors and insulators with a semilocal exchange-correlation potential. *Phys. Rev. Lett.* **102**(22), 226401 (2009)
- [12] Lee, K.-M., Kim, C.M., Sato, S.A., Otobe, T., Shinohara, Y., Yabana, K., Jeong, T.M.: First-principles simulation of the optical response of bulk and thin-film α -quartz irradiated with an ultrashort intense laser pulse. *J. Appl. Phys.* **115**(5), 053519 (2014)
- [13] Brouwer, N., Rethfeld, B.: Transient electron excitation and nonthermal electron-phonon coupling in dielectrics irradiated by ultrashort laser pulses. *Phys. Rev. B* **95**(24), 245139 (2017)
- [14] Sato, S.A., Shinohara, Y., Otobe, T., Yabana, K.: Dielectric response of laser-excited silicon at finite electron temperature. *Phys. Rev. B* **90**(17), 174303 (2014)
- [15] Silaeva, E.P., Bevilion, E., Stoian, R., Colombier, J.P.: Ultrafast electron dynamics and orbital-dependent thermalization in photoexcited metals. *Phys. Rev. B* **98**(9), 094306 (2018)
- [16] Van Overstraeten, R.J., Mertens, R.P.: Heavy doping effects in silicon. *Solid-State Electron.* **30**(11), 1077 (1987)
- [17] Nagai, T., Inagaki, T.J., Kanemitsu, Y.: Band-gap renormalization in highly excited GaN. *Appl. Phys. Lett.* **84**(8), 1284 (2004)
- [18] Gonze, X., Amadon, B., Anglade, P.-M., Beuken, J.-M., Bottin, F., Boulanger, P., Bruneval, F., Caliste, D., Caracas, R., Côté, M., Deutsch, T., Genovese, L., Ghosez, P., Giantomassi, M., Goedecker, S., Hamann, D.R., Hermet, P., Jollet, F., Jomard, G., Leroux, S., Mancini, M., Mazevet, S., Oliveira, M.J.T., Onida, G., Pouillon, Y., Rangel, T., Rignanese, G.-M., Sangalli, D., Shaltaf, R., Torrent, M., Verstraete, M.J., Zerah, G., Zwanziger, J.W.: ABINIT: First-principles approach to material and nanosystem properties. *Comput. Phys. Commun.* **180**(12), 2582 (2009)
- [19] Oshlies, A., Godby, R.W., Needs, R.J.: *GW* self-energy calculations of carrier-induced band-gap narrowing in n-type silicon. *Phys. Rev. B* **51**(3), 1527 (1995)
- [20] Martin-Samos, L., Bussi, G., Ruini, A., Molinari, E., Caldas, M.J.: Unraveling effects of disorder on the electronic structure of SiO₂ from first principles. *Phys. Rev. B* **81**(8), 081202 (2010)
- [21] Kresse, G., Marsman, M., Hintzschke, L.E., Flage-Larsen, E.: Optical and electronic properties of Si₃N₄ and α -sio₂. *Phys. Rev. B* **85**(4), 045205 (2012)
- [22] Yamada, A., Yabana, K.: Energy transfer from intense laser pulse to dielectrics in time-dependent density functional theory. *Eur. Phys. J. D* **73**(5), 87 (2019)
- [23] Bauerhenne, B., Garcia, M.E.: Universal behavior of the band gap as a function of the atomic mean-square displacement in laser-excited silicon. *Adv. Opt. Technol.* **9**(3), 145 (2020)
- [24] Tsaturyan, A., Kachan, E., Stoian, R., Colombier, J.-P.: Ultrafast bandgap narrowing and cohesion loss of photoexcited fused silica. *J. Chem. Phys.* **156**(22), 224301 (2022)

- [25] Derrien, T.J.-Y., Tancogne-Dejean, N., Zhukov, V.P., Appel, H., Rubio, A., Bulgakova, N.M.: Photoionization and transient Wannier-Stark ladder in silicon: First-principles simulations versus Keldysh theory. *Phys. Rev. B* **104**(24), 241201 (2021)